International Journal of Mass Spectrometry 297 (2010) 67–75

Contents lists available at ScienceDirect

International Journal of Mass Spectrometry

journal homepage: www.elsevier.com/locate/ijms

Vibrational spectra of discrete UO_2^{2+} halide complexes in the gas phase

Gary S. Groenewold[a,*], Michael J. van Stipdonk[b], Jos Oomens[c], Wibe A. de Jong[d], Garold L. Gresham[a,1], Michael E. McIlwain[a,1]

[a] Idaho National Laboratory, 2151 North Blvd., Idaho Falls, ID 83402, USA
[b] Wichita State University, Department of Chemistry, 1845 Fairmont Ave, Wichita, KS, USA
[c] FOM Institute for Plasmaphysics, Nieuwegein, The Netherlands
[d] Pacific Northwest National Laboratory, Richland, WA, USA

ARTICLE INFO

Article history:
Received 12 April 2010
Received in revised form 7 June 2010
Accepted 14 June 2010
Available online 20 June 2010

Keywords:
Ion spectroscopy
IRMPD
Coordination complex

ABSTRACT

The intrinsic binding of halide ions to the metal center in the uranyl molecule is a topic of ongoing research interest in both the actinide separations and theoretical communities. Investigations of structure in the condensed phases are frequently obfuscated by solvent interactions that can alter ligand binding and spectroscopic properties. The approach taken in this study is to move the uranyl halide complexes into the gas phase where they are free from solvent interactions, and then interrogate their vibrational spectroscopy using infrared multiple photon dissociation (IRMPD). The spectra of cationic coordination complexes having the composition $[UO_2(X)(ACO)_3]^+$ (where X = F, Cl, Br and I; ACO = acetone) were acquired using electrospray for ion formation, and monitoring the ion signal from the photoelimination of ACO ligands. The studies showed that the asymmetric ν_3 UO_2 frequency was insensitive to halide identity as X was varied from Cl to I, suggesting that in these pseudo-octahedral complexes, changing the nucleophilicity of the halide did not appreciably alter its binding in the complex. The ν_3 peak in the spectrum of the F-containing complex was 9 cm^{-1} lower indicating stronger coordination in this complex. Similarly the ACO carbonyl stretches showed that the C=O frequency was relatively insensitive to the identity of the halide, although a modest shift to higher wavenumber was seen for the complexes with the more nucleophilic anions, consistent with the idea that they loosen solvent binding. Surprisingly, the ν_1 stretch was activated when the softer anions Cl, Br and I were present in the complexes. IR studies of the anionic complexes $[UO_2X_3]^-$ (where X = Cl^-, Br^- and I^-) compared the ν_3 UO_2 modes versus halide, and showed that the ν_3 values decreased with increasing anion nucleophilicity. This observation was consistent with DFT calculations that indicated that $[UO_2X_2]^- – X^\bullet$ and $[UO_2X_2]^\bullet – X^-$ dissociation energies decreased on the order F > Cl > Br > I. The tri-fluoro complex could not be photodissociated in these experiments.

1. Introduction

The intrinsic ligand–metal binding in uranyl coordination complexes is a subject of ongoing research interest because modest differences in complex stability have profound impacts on disposition of the element in actinide separation processes, and in the environment. In particular, halide binding is of interest because uranium halides are used for gaseous separations [1], and because halides affect rates of solvent exchange and hydrolysis [2]. As a result, uranium halide bonding has received significant research interest. Experimentally, uranium halide complexes have been examined using infrared [3,4] and Raman spectroscopy [5], and also X-ray absorption techniques [6]. The linear uranyl cation $[UO_2]^{2+}$ is ideal for measurements because it has intense ν_1 and ν_3 stretching modes that can be readily observed in the Raman and infrared modes, respectively. These vibrations are very sensitive to bonding in the equatorial plane, and as such are sensitive indicators of the chemical environment of the uranium metal atom. These studies have shown that uranium halide binding increases with increasing hardness of the halide anion, with F^- forming the strongest bonds, and I^- the weakest, and that binding strength is inversely related to the uranyl stretching frequencies [3,5].

The sensitivity of the ν_1 and ν_3 vibrational modes to their chemical environment can make interpretation of the spectra complicated, because in addition to the halide ligands, solvent or other neighboring molecules will also affect the uranyl stretching frequencies, making it impossible to distinguish effects of strongly coordinating ligands from those of the solvent. Furthermore, multiple species are always present, as demonstrated by recent X-ray

* Corresponding author. Tel.: +1 208 526 2803; fax: +1 208 526 8541.
E-mail addresses: gary.groenewold@inl.gov, garygroenewold@gmail.com (G.S. Groenewold), michael.vanstipdonk@wsu.edu (M.J. van Stipdonk), joso@rijnh.nl (J. Oomens), wibe.dejong@pnl.gov (W.A. de Jong).
[1] Tel.: +1 208 526 2803.

1387-3806/$ – see front matter © 2010 Elsevier B.V. All rights reserved.
doi:10.1016/j.ijms.2010.06.013

absorption spectroscopy measurements of uranyl chloride in an aqueous-acetonitrile solvent system [7], and probably explains why earlier NMR studies could not identify speciation either [8].

Hence an attractive strategy is to turn to computational chemistry, which has been used to calculate structures, energies and vibrational frequencies of uranium halide complexes [9]. However methods like density functional theory at times encounter difficulty in handling systems with large numbers of electrons, spin orbit coupling and relativistic effects, all of which can be significant in actinide systems. Selection of optimum functionals and basis sets is frequently not straightforward. And the influences of neighboring molecules can make comparison with computational results difficult or impossible, although by employing layered cluster [10] or hybrid DFT-molecular mechanics models this has been achieved [11].

Solvent interactions may be controlled, or eliminated altogether by moving the coordination complexes into the gas phase, where solvent concentrations are much lower or completely absent, and moreover, can be characterized and controlled exactly by mass spectrometry. Using electrospray uranyl halide coordination complexes can be generated [12] and then trapped in a Fourier transform ion cyclotron resonance mass spectrometer, where they can be isolated and then photodissociated using light from a free electron laser (FEL) in the mid-IR [13–15], or from an optical parametric oscillator laser tuned to higher frequencies corresponding to H-stretching regions [16–24]. In the mid-IR region of the spectrum, photons are not sufficiently energetic to cause dissociation needed to observe vibrational fundamentals. However the FEL can deliver sufficient pulse energies so that complexes will absorb multiple photons, and are energized to their dissociation threshold [25]. This approach has been used to examine the IR spectra of a number of metal coordination complexes [13,26–31], and has been applied to uranyl coordination complexes in several studies by our group, specifically $[UO_2(solvent)_n]^{2+}$ [32], $[UO_2(solvent)]^+$ [33], $[UO_2(anion)(solvent)]^+$ [34], and $[UO_2(anion)_3]^-$ complexes [35,36]. These measurements have provided a quantitative basis for evaluating the effects of the number of ligands, and ligand nucleophilicity on binding within the complexes, and have provided a useful basis for comparing the results of theoretical calculations.

In the present study, this experimental strategy is used to investigate uranyl halide complexes having the general composition $[UO_2X(acetone)_3]^+$, and $[UO_2X_3]^-$, where X represents the halide anions. The gas-phase measurements are then compared with those made in the condensed phases, and with theoretical results generated using density functional theory.

2. Experimental

2.1. Materials and methods

2.1.1. Generation of uranyl complexes by ESI

Uranyl halide solutions were generated by first dissolving UO_3 in a slight stoichiometric excess of sulfuric acid, and then adding a barium halide solution to quantitatively precipitate the sulfate as $BaSO_4$. The clouded solution was centrifuged for 1 min to precipitate the salt, which left the uranyl dication in solution with the appropriate halide anion X (X = F, Cl, Br, I). The supernatant was decanted and mixed with MeOH such that the uranyl concentration was 1–2 mM, and this was amended with ~10% acetone (ACO). ESI of these solutions produced the $[UO_2X(ACO)_3]^+$ complexes in the positive ion mode. The cationic bromide and iodide complexes were formed from the same solution, which generated by mixing the supernatants from the respective bromide and iodide uranyl solutions. For the negative ion studies, the uranyl halide solutions were diluted 1:1 with methanol and electrosprayed, which produced a strong signal in the mass spectrum corresponding to $[UO_2X_3]^-$. Spray rates were maintained between 10 and 25 μl/min.

2.1.2. Fourier transform ion cyclotron resonance mass spectrometry (FT-ICR-MS)

Ions were accumulated in an external hexapole for about 500 ms prior to being injected into the ICR cell. The subject anion and cation complexes were isolated for IRMPD study using a stored waveform inverse Fourier transform (SWIFT) pulse [37], which ejected all species except those having the desired mass. To acquire the IR spectra for the $[UO_2Br(ACO)_3]^+$ and $[UO_2I(ACO)_3]^+$ complexes, the SWIFT sequence was set up to isolate both complexes in the same experiment.

2.1.3. Infrared multiple photon dissociation (IRMPD)

In general, infrared spectra of the uranyl complex ions were collected by monitoring the efficiency of IRMPD as a function of photon energy [25]. In this experiment, isolated complexes were irradiated using two FELIX macropulses (40 mJ per macropulse, 5 μs pulse duration, FWHM bandwidth around 0.5% of central λ). When the laser frequency matches that of a normal vibrational mode of the gas-phase ion, energy is absorbed and subsequently distributed throughout the ion by intramolecular vibrational redistribution (IVR). The rapidity of the IVR process allows the energy of each photon to be "relaxed" prior to the absorption of the next, and thus allows promotion of the ion's internal energy to the dissociation threshold by multiple photon absorption [25]. Prior studies have shown that the infrared spectra obtained using the IRMPD method presented here are comparable to those obtained using linear absorption techniques [27,36,38].

To produce infrared spectra, the free electron laser was scanned in 0.01–0.04 μm increments between 6 and 12.5 μm (wavelength was adjusted in linear increments), measuring product ions and un-dissociated precursor ions using the excite/detect sequence of the FT-ICR-MS [39,40] after each IRMPD step. The IRMPD yield was normalized to the summed fragment ion yield, and corrected for variations in FELIX power over the spectral range, and then plotted as $-\log(1 - \text{yield})$.

2.2. Density functional theory calculations

DFT calculations of structures and harmonic frequencies were performed in order to aid frequency assignments. Calculations were principally conducted using the NWChem software [41]. The structures, vibrational modes, and energetics were determined using the B3LYP exchange-correlation functional [42,43]. For U the small core Stuttgart RECP and associated Stuttgart orbital basis sets [44–50] were used. For C, O and H, the valence triple-ζ plus polarization (TZVP) DFT optimized basis sets were used [51]. For F, Cl, Br and I, the aug-cc-pVTZ basis sets were used [52–55], with the Stuttgart 28 electron effective core potential for I [53]. In all cases, spherical basis sets were employed. Some spin-orbit DFT calculations were performed for the Br complexes. For U a new core- and spin-orbit potential with associated basis set was used [56], while the Br atom was described by a 10 electron effective core and spin-orbit potential and an aug-cc-pVTZ basis set [57]. No spin-orbit potential was included for the oxygen atom.

3. Results and discussion

3.1. IRMPD of cationic uranyl complexes

Electrospray of uranyl halide solutions amended with acetone cleanly produced the $[UO_2X(ACO)_3]^+$ complexes that were isolated and irradiated using FELIX to generate the IRMPD spectra. The spectra of $[UO_2F(ACO)_3]^+$ and $[UO_2Cl(ACO)_3]^+$ were acquired in separate

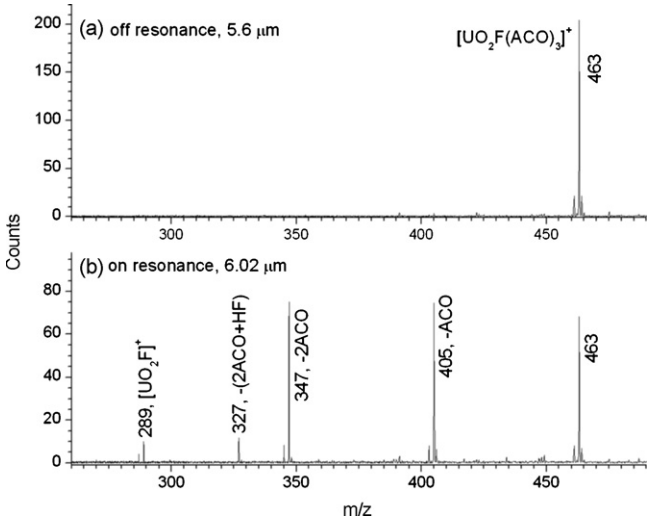

Fig. 1. ESI mass spectra of the uranyl fluoride-acetone solution, after application of a SWIFT pulse to isolate the $[UO_2F(ACO)_3]^+$ complex at m/z 463. (a) Spectrum off resonance at 5.6 μm and (b) on resonance at 6.0 μm.

experiments, while the spectra of the analogous bromide and iodide complexes were acquired in the same experiment from a solution containing uranyl with both anions. This was done to enable collection of the spectra of two complexes from the same experiment, which economized beam time at FELIX.

3.1.1. IRMPD of $[UO_2F(ACO)_3]^+$

The ESI mass spectrum of the uranyl fluoride solution produced an abundant complex at m/z 463 that corresponded to $[UO_2F(ACO)_3]^+$. In addition to the ^{13}C isotopic peak, a small ion at m/z 461 was produced that corresponded to the hydroxide $[UO_2(OH)(ACO)_3]^+$, and this envelope of ions was isolated using a SWIFT sequence [37], and photodissociated with FELIX. Serial elimination reactions result: the complex initially loses one and two ACO ligands to furnish m/z 405 and 347, respectively (Fig. 1). After the second ACO loss, loss of the third ACO generates $[UO_2F]^+$ at m/z 289, and this is competitive with the loss of HF, which forms $[UO_2(ACO–H)]^-$ at m/z 327. The photofragments of the hydroxide complex show up 2 u lower than those of the fluoride complex, which enabled measurement of uranyl ν_3 frequency for the hydroxide [34].

The IRMPD spectrum of the $[UO_2F(ACO)_3]^+$ complex was generated from the summed photodissociation channels corresponding to losses of one and two ACO. An intense peak maximizing at 1667 cm^{-1} corresponds to the C=O stretching mode (Table 1). When the spectra from the individual photodissociation channels are compared, the C=O stretching mode is shifted to lower by 6 cm^{-1} in the (−2 ACO) channel (Fig. 2), which occurs as a result of activation of anharmonic modes. Anharmonic shifts to lower cm^{-1} have been previously noted for higher energy fragmentation reactions [58]. The shift to lower cm^{-1} becomes more significant as dissociation proceeds, i.e., the channel spectra generated from loss of three ACO and (two ACO + HF) have C=O stretching modes that have the largest shifts to lower cm^{-1}. The channel spectrum from the (−1 ACO) is least influenced by the anharmonic modes, however it was of low intensity in the chloride complex (see below). As a compromise between minimizing anharmonic effects and need for reasonable signal-to-noise, the sum of the photodissociation channel spectra from loss of one ACO and two ACO were used for comparisons.

The C=O stretching mode for the $[UO_2F(ACO)_3]^+$ complex is 38 cm^{-1} higher than that reported for the $[UO_2(ACO)_4]^{2+}$ complex [32]. This indicates that substitution of F^- for ACO loosens ACO

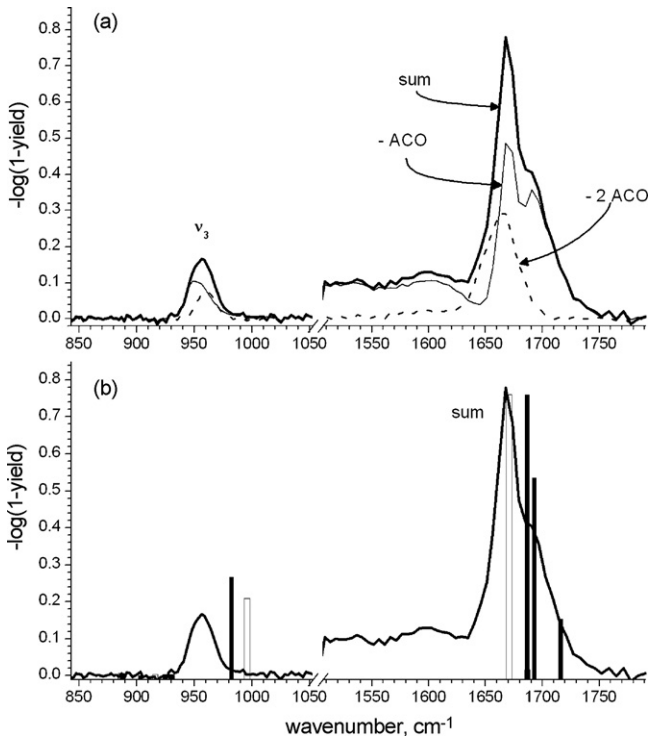

Fig. 2. Infrared multiple photon dissociation spectrum of $[UO_2F(ACO)_3]^+$. (a) Thick black trace is the IRMPD spectrum generated from the sum of the two dissociation channels. Thin and dashed traces are individual dissociation channel spectra for (−1 ACO) and (−2 ACO), respectively and (b) summed dissociation channels, superimposed with DFT-calculated bands. Black columns are bands calculated for $[UO_2F(ACO)_3]^+$, while the open columns are bands calculated for $[UO_2F(ACO)_2]^+$.

binding in the complex, with a concomitant strengthening of the C=O bond. The peak displays a significant tail at lower cm^{-1}, which also is the result of activation of anharmonic modes. The spectrum generated by the (−1 ACO) channel spectrum shows a partially resolved, high frequency shoulder that is ~22 cm^{-1} higher than the most intense carbonyl peak. This suggests that in the intact complex, acetone occupies at least two distinct chemical environments, which is in agreement with DFT calculations that show that the ACO ligand trans to the fluoride is less strongly bound compared to the ACO ligands located cis (see below).

The uranyl ν_3 stretching mode of $[UO_2F(ACO)_3]^+$ was measured at 956 cm^{-1}, and a comparison of the spectral response in the individual fragmentation channels shows that the ν_3 mode is shifted higher by ~10 cm^{-1} in the (−2 ACO) channel compared to that of the (−1 ACO) channel. This trend is counter to that seen for most serial losses, which show a red shift as energetic requirements increase [58] (note that elimination of two ACO ligands is more energetically demanding than elimination of one). The trend suggests that the $[UO_2F(ACO)_2]^+$ intermediate formed by loss of one ACO during the experiment may be contributing to the IRMPD spectrum. This explanation is supported by the DFT calculations (Table 1) and by prior measurements that show that uranyl complexes with fewer equatorial ligands have ν_3 stretching modes at higher cm^{-1} [32,34].

At 956 cm^{-1}, the value for the ν_3 stretching mode consistent with values measured for other ligated uranyl-anion complexes in the gas phase [34,35], but ~50 cm^{-1} higher than that reported by Gal for uranyl fluoride complexes in aqueous solution [3]. The large difference between the gas-phase and solution values is somewhat surprising considering that the acetone ligands bound to the gas-phase complex are expected to be more electron donating than water. The difference also highlights difficulty in correlating solution species and “solvated” species in the gas phase, which

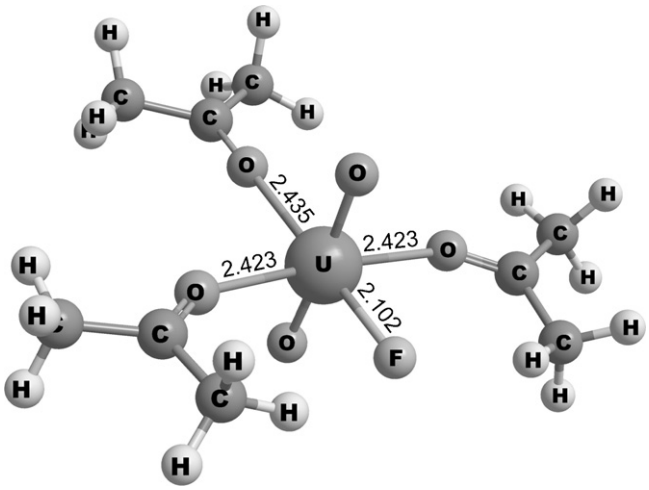

Fig. 3. DFT-calculated structure for $[UO_2F(ACO)_3]^+$. Bond lengths are in Å.

is challenging on account of multiple species in the former, and the absence of the second solvation sphere in the latter. The ν_3 value for uranyl fluoride salts are even lower, ranging from 850 to 908 cm^{-1}, indicative of much stronger or more extensive equatorial coordination for UO_2^{2+} in crystalline environments [4].

Density functional theory calculations (B3LYP functional) for $[UO_2F(ACO)_3]^+$ predict a distorted octahedral structure (Fig. 3). The O=U=O bond angle is slightly bent away from the fluoride ligand at 174.5° (Table 2), which contrasts with most uranyl complexes, in which this bond is closer to linear. The structure provides a slightly different environment for the ACO ligand trans to the fluoride, which has a slightly longer $U–O_{equatorial}$ bond distance (0.012 Å) compared to than those of the two cis-ACO ligands, and a shorter C=O bond with a stretching mode at slightly higher cm^{-1} compared to the cis ligands. The DFT calculation actually predicts three carbonyl bands as indicated by the black columns in Fig. 2b (Table 1) at 1687, 1693, and 1716 cm^{-1}. The band at 1687 cm^{-1} is a mode that only involves the two ACO ligands cis to fluoride (and more tightly bound), while the 1693 and 1716 cm^{-1} modes are coupled vibrations of these two acetones with the acetone trans to the F. On a qualitative basis, the calculations are in agreement with the carbonyl region of the IRMPD spectrum, which also predicts ACO ligands in multiple environments within the $[UO_2F(ACO)_3]^+$ complex.

The DFT calculations also predict the UO_2 ν_3 stretch at 982 cm^{-1} which is 26 cm^{-1} higher than the measurement. A similar discrepancy between the measured and computed values is seen for the carbonyl stretching mode, and overall the calculations over-predict the measured frequencies by 20–30 cm^{-1}. Modest over-prediction of vibrational frequencies is typical for DFT calculations, which are normally scaled by factors ranging from 0.95 to 0.98 to give optimal agreement with IRMPD spectra [59–62].

The DFT calculations add support to the idea that transient $[UO_2F(ACO)_2]^+$ may be contributing to the IRMPD spectrum. Trends in the C=O and antisymmetric O=U=O modes observed in comparing the (−1 ACO) and (−2 ACO) channel spectra are in qualitative agreement with those comparing the same modes in the DFT-calculated spectra of $[UO_2F(ACO)_3]^+$ and $[UO_2F(ACO)_2]^+$, i.e., they show shifts in the same direction and the shifts have similar magnitudes. The value calculated for the C=O stretching mode for $[UO_2F(ACO)_2]^+$ is 16 cm^{-1} lower than that calculated for $[UO_2F(ACO)_3]^+$, and a similar shift is also seen in a comparison of the (−2 ACO) and (−1 ACO) channel spectra. Conversely, the value calculated for the O=U=O antisymmetric mode for $[UO_2F(ACO)_2]^+$ is 14 cm^{-1} higher than that calculated for $[UO_2F(ACO)_3]^+$, and a shift to higher cm^{-1} is seen in the channel spectrum of $[UO_2F(ACO)_2]^+$ when compared to that of $[UO_2F(ACO)_3]^+$.

3.1.2. IRMPD of $[UO_2Cl(ACO)_3]^+$

ESI of the uranyl chloride solution produced abundant ions at m/z 479 and 481 that corresponded to the two chlorine isotopic ions of $[UO_2Cl(ACO)_3]^+$. The more abundant 479 isotopic ion was isolated for the IRMPD experiments (adequate signal-to-noise was achieved without including the ^{37}Cl isotopic ion). Irradiation of $[UO_2Cl(ACO)_3]^+$ at ~6.0 μm (on resonance with the carbonyl stretch) produced the analogous ensemble of photodissociation products as were observed in the fluoride experiments: elimination of one and two acetone (ACO) ligands to produce m/z 421 and 363, followed by competitive losses of HCl and a third ACO, furnishing lower abundance ions at m/z 327 and 305, respectively. A low abundance ion at m/z 287 arises from C_3H_4 loss from $[UO_2(ACO–H)]^+$ (m/z 327), and another low intensity photofragment was observed at m/z 434, which would correspond to loss of 45 u from the parent complex. The origin of this latter species has not been satisfactorily explained, but the overarching behavior is loss of ACO ligands, consistent with the composition and structure of the proposed complex.

Both the carbonyl and uranyl regions of the IR were scanned and the summed IRMPD spectrum was generated by adding (−1 ACO) and (−2 ACO) dissociation channels. The intense carbonyl absorption band was measured at ~1660 cm^{-1} (Fig. 4), and the antisymmetric uranyl ν_3 mode at 965 cm^{-1}. Comparison of the individual channel spectra from the (−1 ACO) and (−2 ACO) eliminations reveals trends similar to those seen in the spectra of the fluoride complex. The carbonyl stretching mode in the (−2 ACO) channel spectrum was ~20 cm^{-1} lower than in the spectrum of the (−1 ACO) channel, consistent with a modest anharmonic shift [58]. The carbonyl bands generated by the (−3 ACO) and (−2 ACO–HCl) channel spectra are lower still. The trend is reversed in the uranyl asymmetric ν_3 mode, with the peak in the (−2 ACO) channel spectrum ~2 cm^{-1} higher than in the (−1 ACO) channel. As in the case of the fluoride complex, this suggests contribution from dissociation of the intermediate $[UO_2Cl(ACO)_2]^+$ complex. In addition, a very low abundance peak is seen at 881 cm^{-1}, which corresponds to the symmetric uranyl ν_1 stretching mode and suggests distortion of the uranyl molecule. The ν_1 stretching mode is only seen in the (−1 ACO) channel spectrum, and the low intensity suggests that photodissociation of the molecule via the ν_1 mode is inefficient, and hence energy that is deposited into this mode is only sufficient to cause the lowest energy fragmentations. The ν_1 mode is likely not active in the (−2 ACO) channel if the $[UO_2Cl(ACO)_2]^+$

Table 1
Vibrational frequencies measured in the IRMPD experiments, and calculated using DFT. Note that calculated values for both the $(ACO)_3$ and $(ACO)_2$ complexes are provided.

X	O=U=O ν_3 stretch			ACO C=O stretch		
	IRMPD, $[UO_2X(ACO)_3]^+$	DFT, $[UO_2X(ACO)_3]^+$	DFT, $[UO_2X(ACO)_2]^+$	IRMPD, $[UO_2X(ACO)_3]^+$	DFT, $[UO_2X(ACO)_3]^+$	DFT, $[UO_2X(ACO)_2]^+$
F	956	982	996	1667	1687, 1693, 1716	1671
Cl	965	992	1004	1660	1685, 1690, 1716	1666
Br	966	990	1004	1668	1675, 1688, 1711	1667
I	966	989	1003	1673	1670, 1687, 1710	1669

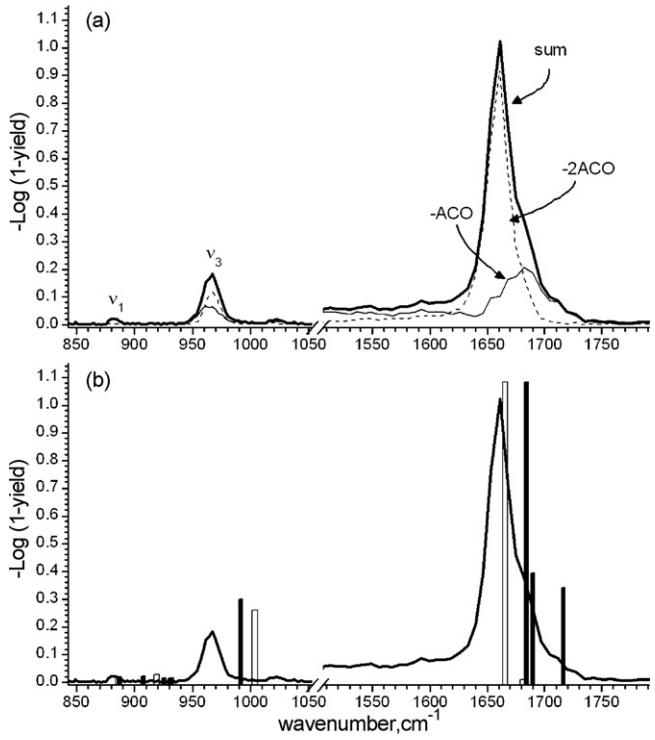

Fig. 4. Infrared multiple photon dissociation spectrum of $[UO_2Cl(ACO)_3]^+$. (a) Thick black trace is the IRMPD spectrum generated from the sum of the two dissociation channels. Thin and dashed traces are the individual dissociation channel spectra for the (−1 ACO) and (−2 ACO) eliminations, respectively and (b) summed IRMPD spectrum, superimposed with DFT-calculated bands. Black columns are bands calculated for $[UO_2Cl(ACO)_3]^+$, while the open columns are bands calculated for $[UO_2Cl(ACO)_2]^+$.

complex participates, because the uranyl molecule is more linear in this complex. This explanation is consistent with the high baseline in the 1500–1600 cm^{-1} region of the (−1 ACO) channel spectrum, where the molecule is undergoing inefficient anharmonic photodissociation. The effect diminishes as the energy required for photodissociation increases.

The uranyl ν_3 mode for the $[UO_2Cl(ACO)_3]^+$ complex was measured at 965 cm^{-1}, a value that was in very close agreement with values reported for aqueous uranyl chloride complexes (962 and 956 cm^{-1}) [3], although the explicit speciation was not known in the condensed phase studies. The IRMPD value was significantly higher than that reported for the di-anionic tetrachloro-complex $[UO_2Cl_4]^{2-}$, where a value of 918 cm^{-1} measured for a solution of tetramethylammonium uranyl tetrachloride in CH_2Cl_2 [4]. The value was 9 cm^{-1} higher than that measured in the IRMPD spectrum of the $[UO_2F(ACO)_3]^+$ complex, suggesting that the axial uranyl oxo ligands are slightly stronger in the chloride complex.

The DFT structure of the $[UO_2Cl(ACO)]^+$ complex is a distorted octahedron that was very similar to that calculated for the fluoride complex. The uranyl O=U=O bond angle is 172.99° with the axial oxygen atoms bent away from the chloride ligand (Table 2). The two ACO ligands that are cis to the chloride have identical U–$O_{equatorial}$ bond lengths of 2.406 Å, respectively. The trans-ACO ligand is more loosely bound, with a U–$O_{equatorial}$ bond length of 2.431 Å. These bonds are slightly shorter than those calculated for the ACO ligands in the fluoride complex, as are the U–O_{axial} bonds, observations consistent with looser binding of chloride compared to fluoride.

The calculated IR spectrum of the $[UO_2Cl(ACO)_3]$ complex contains three distinct carbonyl bands that are higher the measurements by 25–56 cm^{-1}, indicative of multiple chemical environments for the ACO ligands. While cleanly resolved carbonyl absorption bands were not observed in the IRMPD spectrum, the peak in this region of the spectrum is broadened in a manner consistent with non-resolved, overlapping peaks. The calculated carbonyl bands were also slightly lower than calculated values for the corresponding fluoride complex, indicating that the ACO ligands are more strongly bound in the $[UO_2Cl(ACO)_3]^+$ complex. The calculated uranyl ν_3 band was 10 cm^{-1} higher than that calculated for the fluoride complex, a difference that is in excellent agreement with the IRMPD values. The higher uranyl ν_3 band indicates that the axial oxo ligands are more strongly bound as a result of less electron density donated to the metal center by the equatorial ligands in the chloride complex. Photodissociation of the $[UO_2Cl(ACO)_2]^+$ complex may contribute a fraction of the overall signal seen in the IRMPD spectrum of the tris-ACO complex, and could explain the shift to higher cm^{-1} seen in comparing the (−2 ACO) channel spectrum with that of the (−1 ACO) channel (a phenomenon similar to that seen in the fluoride complex).

3.1.3. IRMPD of $[UO_2(Br)(ACO)_3]^+$

The $[UO_2Br(ACO)_3]^+$ complex was generated together with the corresponding iodide complex from a ESI of a solution containing both anions. Both of the bromine isotopic ions were utilized in the IRMPD experiments. $[UO_2Br(ACO)_3]^+$ undergoes photodissociation by serial losses of one, two and three acetone ligands. Serial elimination of a bromine radical furnish both $[UO_2(ACO)]^+$ and $[UO_2]^+$ but these photofragments were not used to generate the IR spectrum, because their spectra were expected to have strong anharmonic shifts, and more importantly because these ions could also be formed from the iodide complex, whose spectrum was collected in the same experiment. This meant that photofragmentation peaks of the bromide and iodide complexes that were generated by the $[UO_2(ACO)]^+$ and $[UO_2]^+$ dissociation channels could not be differentiated.

The carbonyl stretching mode was recorded as a broadened peak from about 1660 to 1700 cm^{-1}, maximizing at 1668 cm^{-1}. The broadened appearance is most likely the result of (a) contributions from multiple carbonyl bands as indicated by the DFT calculations (see below), and (b) differences in the (−1 ACO) and (−2 ACO) channel spectra that were used to generate the summed IRMPD spectrum shown in Fig. 5. Because the signal-to-noise ratio in this spectrum is not as high as in other measurements, there is a possibility that the broadened peak could be due to noise and not multiple bands. This explanation is less likely however, because other bands that are not overlapped (i.e., the uranyl ν_3) do not display significant broadening. The peak maximum was within 8 cm^{-1} of values measured for the three analogous halide–tris-ACO complexes, indicating that binding of acetone is very similar in all four

Table 2
DFT-calculated bond lengths (Å) and angles for $[UO_2X(ACO)_3]^+$. In the fluoride and chloride complexes, the cis-ACO ligands have identical U–O_{eq} bond lengths.

Bond/angle	$[UO_2F(ACO)_3]^+$	$[UO_2Cl(ACO)_3]^+$	$[UO_2Br(ACO)_3]^+$	$[UO_2I(ACO)_3]^+$
U–O_{axial}	1.771 Å	1.765 Å	1.763, 1.767 Å	1.763, 1.767 Å
U–O_{eq}, cis to X	2.423 Å	2.406 Å	2.396, 2.430 Å	2.394, 2.433 Å
U–O_{eq}, trans to X	2.435 Å	2.431 Å	2.424 Å	2.422 Å
U–X	2.102 Å	2.587 Å	2.751 Å	2.982 Å
O–U–O angle	174.5°	173.9°	174.0°	174.1°

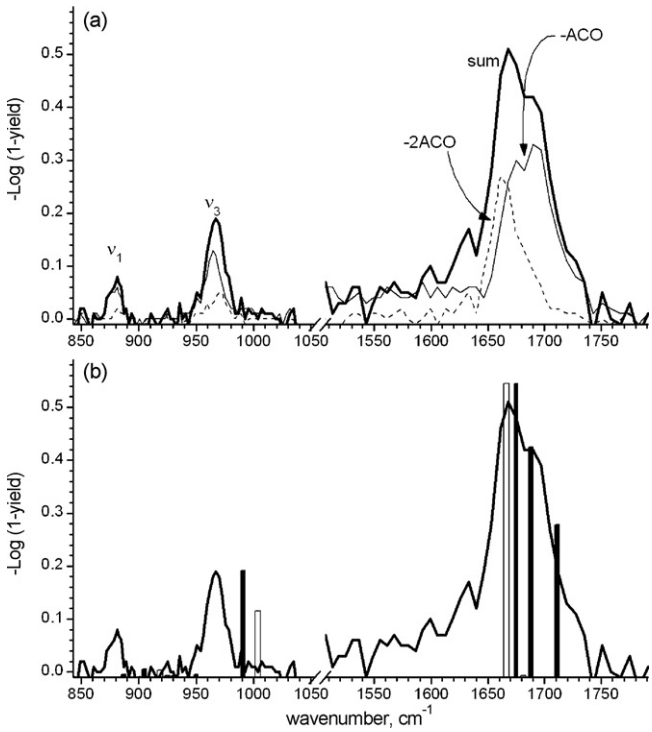

Fig. 5. Infrared multiple photon dissociation spectrum of $[UO_2Br(ACO)_3]^+$. (a) Thick black trace is the IRMPD spectrum generated from the sum of the two dissociation channels. Thin and dashed traces are the individual dissociation channel spectra for the (−1 ACO) and (−2 ACO) eliminations, respectively and (b) summed IRMPD spectrum, superimposed with DFT-calculated bands. Black columns are bands calculated for $[UO_2Br(ACO)_3]^+$, while the open columns are bands calculated for $[UO_2Br(ACO)_2]^+$.

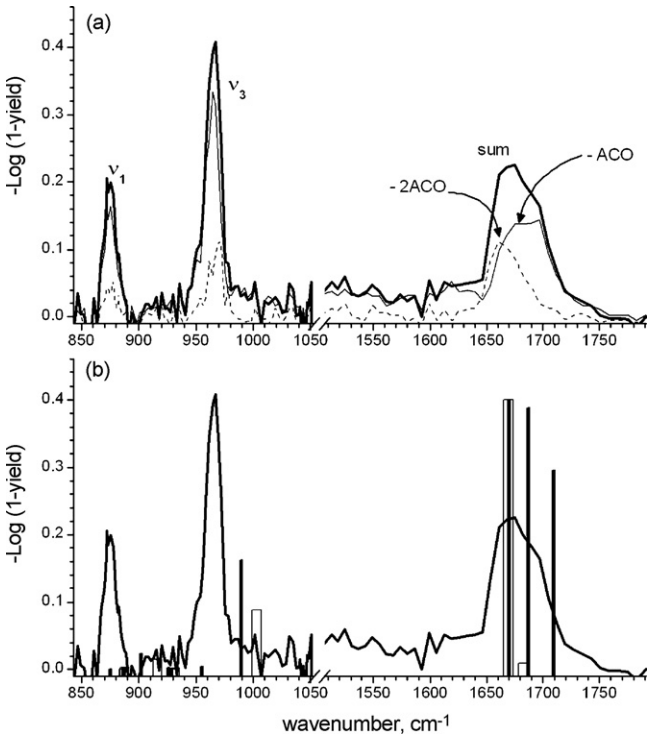

Fig. 6. Infrared multiple photon dissociation spectrum of $[UO_2I(ACO)_3]^+$. (a) Thick black trace is the IRMPD spectrum generated from the sum of the two dissociation channels. Thin and dashed traces are the individual dissociation channel spectra for the (−1 ACO) and (−2 ACO) eliminations, respectively and (b) summed IRMPD spectrum, superimposed with DFT-calculated bands. Black columns are bands calculated for $[UO_2I(ACO)_3]^+$, while the open columns are bands calculated for $[UO_2I(ACO)_2]^+$.

complexes. Comparing carbonyl stretching bands recorded in the two dissociation channel spectra, (−2 ACO) channel was shifted to lower cm^{-1} compared to the (−1 ACO) channel, suggesting anharmonicity in the former channel that is consistent with increased dissociation energy needed to eliminate two ACO ligands. The carbonyl peak in the (−1 ACO) channel spectrum has two maxima separated by ∼17 cm^{-1}, suggesting two or more bands, a conclusion in agreement with the DFT spectrum.

The DFT-calculated spectrum has three significant carbonyl bands (Fig. 5b) arising from different carbonyl environments and mode coupling. The structure predicted for the $[UO_2Br(ACO)_3]^+$ complex is again a distorted octahedron, but with less symmetry than either the F or Cl versions, in that the two ACO ligands cis- to the Br^- are non-equivalent: one ACO has a U–O_{eq} bond distance of 2.430 Å, while the other cis-ACO is shorter, at 2.396 Å (Table 2). The trans-ACO ligand was intermediate between these values, at 2.424 Å. The modeled structure shows that in addition, the most loosely held cis-ACO situated out of the equatorial plane, indicating that ligand repulsion is beginning to influence the structure. Like the F and Cl complexes, the uranyl bond is slightly bent with a O=U=O bond angle of 174.0°, with the oxo ligands bent away from the bromide.

The uranyl ν_3 band was measured at 966 cm^{-1}, a value nearly identical to that of both the chloride and iodide complexes, and 10 cm^{-1} higher than that of the fluoride complex. There were differences between the individual fragment channel spectra, with the peak in the (−1 ACO) channel being about 5 cm^{-1} lower than that in the (−2 ACO) channel spectrum. This suggests a contribution from photodissociation of the $[UO_2Br(ACO)_2]^+$ intermediate for the same reasons mentioned in the discussions of the Cl and F complexes, where the same trend was seen. As in the case of the chloride, a low abundance peak was measured at 880 cm^{-1}, which corresponds to the ν_1 stretching mode that is activated due to the non-linearity of the uranyl molecule.

3.1.4. IRMPD of $[UO_2I(ACO)_3]^+$

Dissociation of the $[UO_2I(ACO)_3]^+$ complex principally occurred by the elimination of one and two ACO ligands. These losses are followed by serial elimination of an iodine radical to produce $[UO_2(ACO)]^+$, and then another ACO to furnish $[UO_2]^+$. These latter photofragment ions cannot be differentiated from identical ions formed from the bromide complex, which was simultaneously examined in this experiment. The IRMPD spectrum generated from the summed (−1 ACO) and (−2 ACO) photodissociation channels displayed a broad carbonyl absorption band maximizing at about 1673 cm^{-1} (Fig. 6). The (−1 ACO) channel spectrum was also broad without a well-defined peak top, suggesting that it is derived from at least a couple of unresolved carbonyl stretching bands. The (−2 ACO) channel spectrum had a more narrow peak shape, and was ∼20 cm^{-1} lower, consistent with anharmonic shifting as suggested for the other halide complexes above. Compared to the carbonyl frequencies of the other complexes, those of the iodide complex were recorded at slightly higher cm^{-1}, suggesting that the ACO ligands are less tightly bound in $[UO_2I(ACO)_3]^+$.

The peak corresponding to the uranyl ν_3 mode is exactly where it was in the Br complex at 966 cm^{-1}. The uranyl ν_3 peak in the (−2 ACO) channel spectrum is several cm^{-1} higher than in the (−1 ACO) channel. This shift is not consistent with anharmonicity, but instead suggests absorption by the intermediate $[UO_2I(ACO)_2]^+$.

The structure calculated for the $[UO_2I(ACO)_3]^+$ complex is a distorted octahedron, similar to that of the bromide complex with a slightly bent O=U=O moiety (a bond angle of 174.1°, Table 2). As with the bromide complex, the two ACO ligands cis- to the halide are non-equivalent, with the more loosely bound ACO rotated out

Table 3
Uranyl ν_3 frequencies measured and calculated for the $[UO_2X_3]^-$ complexes.

Complex	Dissociation path	IRMPD frequency	B3LYP frequency
$[UO_2F_3]^-$	Not measured	Not measured	927 cm^{-1}
$[UO_2Cl_3]^-$	$\rightarrow [Cl]^- + UO_2Cl_2$, 100%	935 cm^{-1}	975 cm^{-1}
$[UO_2Br_3]^-$	$\rightarrow [Br]^- + UO_2Br_2$, 15%$\rightarrow [UO_2Br_2]^- + Br^\bullet$, 85%	941 cm^{-1}	981 cm^{-1}
$[UO_2I_3]^-$	$\rightarrow [UO_2I_2]^- + I^\bullet$, 100%	948 cm^{-1}	987 cm^{-1}

of the equatorial plane. The calculations show that the multiple ACO environments give rise to three significant carbonyl stretching bands that are separated from one another by 23 and 17 cm^{-1} (Fig. 6b). This spread is consistent with the broadened carbonyl peak in the IRMPD spectrum. Any contribution to the carbonyl peak from the intermediate $[UO_2I(ACO)_2]^+$ complex would be difficult to observe experimentally, because it is predicted to be very nearly equivalent to the low frequency carbonyl peak in the tris-ACO complex. The calculated uranyl ν_3 stretching mode was 23 cm^{-1} higher than the IRMPD measurement. Like the measurements, there was very little difference between the calculated ν_3 frequencies for the Cl, Br and I complexes.

3.2. IRMPD of anionic uranyl complexes

In the negative ion spectrum, anionic uranyl tri-halide complexes $[UO_2X_3]^-$ were formed in abundance for all four halides. These were isolated and photofragmented using FELIX to generate IRMPD spectra, collecting only the spectral region around the uranyl ν_3 vibration. Different photofragmentation behavior was noted in comparing the four complexes. $[UO_2F_3]^-$ could not be photofragmented in this study, which suggests that it is significantly more tightly bound compared to the other three tri-halo complexes, or less likely but also possible is inefficient trapping of the light F^- photofragment. $[UO_2Cl_3]^-$ dissociates solely by loss of neutral UO_2Cl_2 forming chloride as the ionic product. Conversely the tri-iodo complex only eliminates an iodine radical, forming $[UO_2I_2]^-$ in which the metal is reduced to the +5 oxidation state. Interestingly, the tri-bromo complex is intermediate, eliminating both a neutral Br radical, and UO_2Br_2.

The uranyl ν_3 stretching bands measured for the three dissociating complexes range from 935 cm^{-1} for the tri-chloro complex to 948 cm^{-1} for the tri-iodo, with the tri-bromo being intermediate at 941 cm^{-1} (Fig. 7 and Table 3). The value for the $[UO_2Cl_3]^-$ complex was 17 cm^{-1} higher than that reported in solution for $[UO_2Cl_4]^{2-}$ [4]. Fewer equatorial donor ligands result in lower electron density at the metal center, and higher values for the uranyl ν_3 band [32,63,64]. A comparison of the values for the ν_3 stretching modes for the three complexes shows an analogous trend with increasing halide nucleophilicity: the ν_3 values decrease in the order $[UO_2I_3]^- > [UO_2Br_3]^- > [UO_2Cl_3]^-$ (Fig. 7), consistent with progressively stronger halide binding, and concomitant repulsion of the axial oxo ligands.

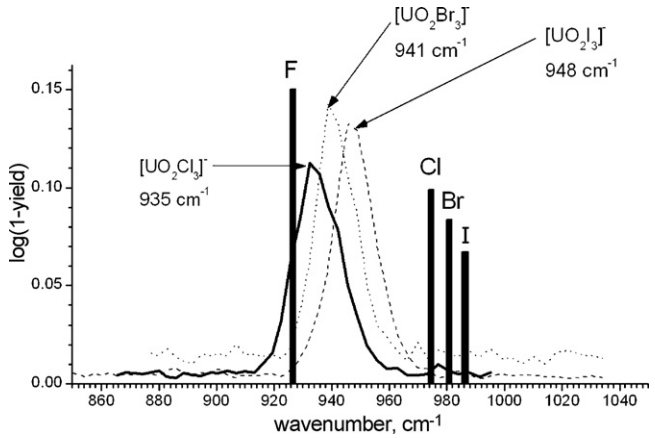

Fig. 7. Infrared multiple photon dissociation spectra of $[UO_2X(ACO)_3]^+$ (lines) plotted with the B3LYP calculated frequencies (columns). Note that the tri-fluoro complex did not dissociate under FELIX irradiation.

Table 4
Structural parameters calculated for the $[UO_2X_3]^-$ complexes.

Bond	$[UO_2F_3]^-$	$[UO_2Cl_3]^-$	$[UO_2Br_3]^-$	$[UO_2I_3]^-$
$U–O_{axial}$	1.796 Å	1.769 Å	1.765 Å	1.762 Å
U–X	2.162 Å	2.649 Å	2.814 Å	3.042 Å

Table 5
Reaction energies calculated for the competing dissociation channels possible in the photodissociation of the $[UO_2X_3]^-$ complexes.

Reaction, partition percentage	ΔE (kcal/mol)
$[UO_2F_3]^- \rightarrow [F]^- + UO_2F_2$, 100%	99.8
$[UO_2F_3]^- \rightarrow [UO_2F_2]^- + F^\bullet$, 0%	124.7
$[UO_2Cl_3]^- \rightarrow [Cl]^- + UO_2Cl_2$, 100%	74.3
$[UO_2Cl_3]^- \rightarrow [UO_2Cl_2]^- + Cl^\bullet$, 0%	87.6
$[UO_2Br_3]^- \rightarrow [Br]^- + UO_2Br_2$, 15%	68.1
$[UO_2Br_3]^- \rightarrow [UO_2Br_2]^- + Br^\bullet$, 85%	74.8
$[UO_2I_3]^- \rightarrow [I]^- + UO_2\ I_2$, 0%	60.7
$[UO_2I_3]^- \rightarrow [UO_2\ I_2]^- + Br^\bullet$, 100%	54.7

For all three anionic complexes the DFT-calculated structures were trigonal bipyramids. The calculated values for the uranyl ν_3 stretching modes were higher than the measurements by ~40 cm^{-1} which would suggest that in these complexes a more significant scaling factor (~0.96) would be required. The accuracy of these calculations is somewhat lower than those performed for the cationic complexes (IRMPD/DFT ratios are between 0.97 and 0.98). The reasons for the difference have not yet been identified but are a topic of further research by our group. On the other hand, the trend in the ν_3 modes is well reproduced by the DFT calculations, as are differences between the halide complexes which are 6–7 cm^{-1} for both the calculations and measurements. The trend is reflected in bond lengths calculated for the structures of the tri-halo complexes, which show a shortening of the $U–O_{axial}$ bond in the order $[UO_2F_3]^- > [UO_2Cl_3]^- > [UO_2Br_3]^- > [UO_2I_3]^-$ (Table 4).

The DFT calculations also provided an estimate of the energetic differences between the two possible dissociation channels that were observed in the photodissociation experiments. B3LYP calculations with the basis set combinations in Section 2 and not including spin-orbit coupling predict an energetic preference for the observed pathway in all cases, with the exception of the tri-bromo complex, which should prefer elimination of neutral UO_2Br_2 by 6.8 kcal/mol (Table 5). When the energetics for the tri-bromo complex were recalculated with spin-orbit coupling included, elimination of the Br radical was predicted to be lower in energy by 1.1 kcal/mol, a difference that is within the accuracy of the methods, and consistent with the experimental observation, i.e., both channels (loss of Br radical and loss of Br^-) are energetically competitive.

4. Conclusions

Infrared multiple photon dissociation spectroscopy of two different types of uranyl halide complexes was used to systematically evaluate the effect of variations in the halide series on vibrations of the complexes. Electrospray ionization produced complexes having the composition $[UO_2X(ACO)_3]^+$ where X = F, Cl, Br, and I, and ACO = acetone. Irradiation using a free electron laser caused extensive dissociation typified by initial losses of one and two ACO ligands that were followed by losses of an additional ACO, HX, and or X radical. Examination of the carbonyl peak in the spectra of individual dissociation channels showed that the more energetically demanding reactions were increasingly anharmonically shifted to lower cm^{-1}. The peaks corresponding to the carbonyl stretching modes were measured at very nearly the same value for all four complexes (peak maxima ranged from 1660 to 1673 cm^{-1}). The carbonyl modes were broadened by ACO ligands are in non-equivalent positions in the complexes, mode coupling, and anharmonicity effects.

The uranyl ν_3 stretching mode was measured and found to be relatively insensitive to variation of the halide, occurring from 965 to 966 cm^{-1} for the Cl, Br and I containing complexes. These values are consistent with previous IRMPD measurements of solvated ion pairs [34]. The exception is the fluoride complex, which has a ν_3 frequency somewhat lower at 956 cm^{-1}, indicating stronger coordination in this case. The ν_3 values are not as low as those measured in solution for solvated uranyl halide complexes [3,4], suggesting that the uranyl molecule is more extensively coordinated in solution.

The symmetric ν_1 mode is activated in the $[UO_2X(ACO)_3]^+$ complexes containing Cl, Br and I, which would be consistent with the DFT-calculated structures that show a bent O=U=O bond ($\sim$174°). However this explanation is not in accord with the fact that the calculations also predict a bent uranyl bond for the fluoro complex, whose IRMPD spectrum does not display a peak corresponding to the ν_1 mode. It may be that the ν_1 mode is not activated in the fluoride complex, however resolution of this issue will require additional experimental/theoretical endeavors.

The tri-halo anion complexes $[UO_2X_3]^-$ were also formed by electrospray and characterized by their uranyl ν_3 frequencies. The halogen systematically affects the ν_3 peak, with frequency values decreasing in the order I > Br > Cl, by 6–7 cm^{-1} for each step. The tri-fluoro complex could not be measured, presumably because it is very strongly coordinated and hence reluctant to fragment. The tri-chloro complex dissociated by the elimination of UO_2Cl_2 forming $[Cl]^-$ as the ionic photofragment. The dissociation pathway switches in the tri-iodo complex, which only dissociates by loss of an iodine radical, forming $[UO_2I_2]^-$. Both processes occur in the tri-bromo complex, i.e., both the Br radical and UO_2Br_2 are eliminated. Energetic trends are accurately predicted for these processes by the DFT calculations, however detailed inclusion of spin orbit coupling effects is needed for the $[UO_2Br_3]^-$ complex in order to get results that are in accord with the competitive elimination pathways.

Acknowledgments

Work by G.S. Groenewold, G.L. Gresham and M.E. McIlwain was supported by the U.S. Department of Energy, Assistant Secretary for Environmental Management, and the INL Laboratory Directed Research & Development Program under DOE Idaho Operations Office Contract DE-AC07-05ID14517. M.J. Van Stipdonk was supported through a grant from the U.S. National Science Foundation (NSF grant CAREER-0239800). J. Oomens was supported by the Nederlandse Organisatie voor Wetenschappelijk Onderzoek (NWO). The skillful assistance by the FELIX staff, in particular Dr. B. Redlich, is gratefully acknowledged. Construction and shipping of the FT-ICR-MS instrument was made possible through funding from the National High Field FT-ICR Facility (grant CHE-9909502) at the National High Magnetic Field Laboratory, Tallahassee, FL. A portion of W.A. de Jong's research was performed using EMSL, a national scientific user facility sponsored by the Department of Energy's Office of Biological and Environmental Research and located at Pacific Northwest National Laboratory.

Appendix A. Supplementary data

Supplementary data associated with this article can be found, in the online version, at doi:10.1016/j.ijms.2010.06.013.

References

[1] R.S. Kemp, Sci. Global Secur. 16 (2008) 115.
[2] I. Farkas, I. Banyai, Z. Szabo, U. Wahlgren, I. Grenthe, Inorg. Chem. 39 (2000) 799.
[3] M. Gal, P.L. Goggin, J. Mink, J. Mol. Struct. 114 (1984) 459.
[4] M. Gal, P.L. Goggin, J. Mink, Spectrochim. Acta 48A (1992) 121.
[5] C. Nguyen-Trung, G.M. Begun, D.A. Palmer, Inorg. Chem. 31 (1992) 5280.
[6] C. Den Auwer, E. Simoni, S. Conradson, C. Madic, Eur. J. Inorg. Chem. (2003) 3843.
[7] C. Hennig, K. Servaes, P. Nockemann, K. Van Hecke, L. Van Meervelt, J. Wouters, L. Fluyt, C. Gorrller-Walrand, R. Van Deun, Inorg. Chem. 47 (2008) 2987.
[8] A. Fratiello, V. Kubo, R.E. Lee, R.E. Schuster, J. Phys. Chem. 74 (1970) 3726.
[9] G.A. Shamov, G. Schreckenbach, T.N. Vo, Chem. Eur. J. 13 (2007) 4932.
[10] S. Matsika, R.M. Pitzer, J. Phys. Chem. A 105 (2001) 637.
[11] I. Infante, L. Visscher, J. Comput. Chem. 25 (2004) 386.
[12] V. Anbalagan, W. Chien, G.L. Gresham, G.S. Groenewold, M.J. Van Stipdonk, Rapid Commun. Mass Spectrom. 18 (2004) 3028.
[13] J.J. Valle, J.R. Eyler, J. Oomens, D.T. Moore, A.F.G. van der Meer, G. von Helden, G. Meijer, C.L. Hendrickson, A.G. Marshall, G.T. Blakney, Rev. Sci. Instrum. 76 (2005) 023103.
[14] D.T. Moore, J. Oomens, L. van der Meer, G. von Helden, G. Meijer, J. Valle, A.G. Marshall, J.R. Eyler, ChemPhysChem 5 (2004) 740.
[15] D. Oepts, A.F.G. van der Meer, P.W. van Amersfoort, Infrared Phys. Technol. 36 (1995) 297.
[16] P.D. Carnegie, B. Bandyopadhyay, M.A. Duncan, J. Phys. Chem. A 112 (2008) 6237.
[17] M.A. Duncan, Annu. Rev. Phys. Chem. 48 (1997) 69.
[18] M.A. Duncan, Int. Rev. Phys. Chem. 22 (2003) 407.
[19] T.D. Jaeger, M.A. Duncan, J. Phys. Chem. A 109 (2005) 3311.
[20] E.D. Pillai, T.D. Jaeger, M.A. Duncan, J. Phys. Chem. A 109 (2005) 3521.
[21] E.D. Pillai, T.D. Jaeger, M.A. Duncan, J. Am. Chem. Soc. 129 (2007) 2297.
[22] A.C. Scott, N.R. Foster, G.A. Grieves, M.A. Duncan, Int. J. Mass Spectrom. 263 (2007) 171.
[23] R.S. Walters, E.D. Pillai, M.A. Duncan, J. Am. Chem. Soc. 127 (2005) 16599.
[24] G. Gregoire, M.A. Duncan, J. Chem. Phys. 117 (2002) 2120.
[25] V.N. Bagratashivili, V.S. Letokov, A.A. Makarov, E.A. Ryabov, Multiple Photon Infrared Laser Photophysics and Photochemistry, Harwood, Chur, Switzerland, 1985.
[26] D.T. Moore, J. Oomens, J.R. Eyler, G. Meijer, G. von Helden, D.P. Ridge, J. Am. Chem. Soc. 126 (2004) 14726.
[27] J. Oomens, D.T. Moore, G. von Helden, G. Meijer, R.C. Dunbar, J. Am. Chem. Soc. 126 (2004) 724.
[28] R.C. Dunbar, D.T. Moore, J. Oomens, J. Phys. Chem. A 110 (2006) 8316.
[29] R.C. Dunbar, D.T. Moore, J. Oomens, Int. J. Mass Spectrom. 265 (2007) 182.
[30] N. Polfer, J. Oomens, R.C. Dunbar, ChemPhysChem 9 (2008) 579.
[31] J. Lemaire, P. Boissel, M. Heninger, G. Mauclaire, G. Bellec, H. Mestdagh, A. Simon, S. Le Caer, J.M. Ortega, F. Glotin, P. Maitre, Phys. Rev. Lett. 89 (2002).
[32] G.S. Groenewold, A.K. Gianotto, K.C. Cossel, M.J. Van Stipdonk, D.T. Moore, N. Polfer, J. Oomens, W.A. de Jong, L. Visscher, J. Am. Chem. Soc. 107 (2006) 4802.
[33] G.S. Groenewold, M.J. van Stipdonk, W.A. de Jong, J. Oomens, G.L. Gresham, M.E. McIlwain, D. Gao, B. Siboulet, L. Visscher, M. Kullman, N. Polfer, ChemPhysChem 9 (2008) 1278.
[34] G.S. Groenewold, A.K. Gianotto, M.E. McIlwain, M.J. Van Stipdonk, M. Kullman, D.T. Moore, N. Polfer, J. Oomens, I. Infante, L. Visscher, B. Siboulet, W.A. De Jong, J. Phys. Chem. A 112 (2008) 508.
[35] G.S. Groenewold, W.A. de Jong, J. Oomens, M.J. Van Stipdonk, J. Am. Soc. Mass Spectrom. 21 (2010) 719.
[36] G.S. Groenewold, J. Oomens, W.A. de Jong, G.L. Gresham, M.E. McIlwain, M.J. Van Stipdonk, PhysChemChemPhys 10 (2008) 1192.
[37] A.G. Marshall, T.-C.L. Wang, T.L. Ricca, J. Am. Chem. Soc. 107 (1985) 7893.
[38] J. Oomens, A.G.G.M. Tielens, B.G. Sartakov, G. Von Helden, G. Meijer, Astrophys. J. 591 (2003) 968.
[39] A.G. Marshall, Acc. Chem. Res. 18 (1985) 316.
[40] A.G. Marshall, C.L. Hendrickson, G.S. Jackson, Mass Spectrom. Rev. 17 (1998) 1.

[41] R.A. Kendall, E. Apra, D.E. Bernholdt, E.J. Bylaska, M. Dupuis, G.I. Fann, R.J. Harrison, J. Ju, J.A. Nichols, J. Nieplocha, T.P. Straatsma, T.L. Windus, A.T. Wong, Comput. Phys. Commun. 128 (2000) 260.
[42] A.D. Becke, J. Chem. Phys. 98 (1993) 5648.
[43] C.T. Lee, W.T. Yang, R.G. Parr, Phys. Rev. B 37 (1988) 785.
[44] A. Bergner, M. Dolg, W. Kuchle, H. Stoll, H. Preuss, Mol. Phys. 80 (1993) 1431.
[45] M. Dolg, H. Stoll, H. Preuss, R.M. Pitzer, J. Phys. Chem. 97 (1993) 5852.
[46] P. Fuentealba, H. Preuss, H. Stoll, L. Vonszentpaly, Chem. Phys. Lett. 89 (1982) 418.
[47] P. Fuentealba, L. Vonszentpaly, H. Preuss, H. Stoll, J. Phys. B: Atom. Mol. Opt. Phys. 18 (1985) 1287.
[48] G. Igel-Mann, H. Stoll, H. Preuss, Mol. Phys. 65 (1988) 1321.
[49] W. Kuchle, M. Dolg, H. Stoll, H. Preuss, Mol. Phys. 74 (1991) 1245.
[50] W. Kuchle, M. Dolg, H. Stoll, H. Preuss, J. Chem. Phys. 100 (1994) 7535.
[51] N. Godbout, D.R. Salahub, J. Andzelm, E. Wimmer, Can. J. Chem. -Rev. Can. Chim. 70 (1992) 560.
[52] T.H. Dunning, J. Chem. Phys. 90 (1989) 1007.
[53] K.A. Peterson, B.C. Shepler, D. Figgen, H. Stoll, J. Phys. Chem. A 110 (2006) 13877.
[54] A.K. Wilson, S.E. Woon, K.A. Peterson, J.T.H. Dunning, J. Chem. Phys. 110 (1999) 7667.
[55] D.E. Woon, J.T.H. Dunning, J. Chem. Phys. 98 (1993) 1358.
[56] M. Dolg, X. Cao, J. Phys. Chem. A 113 (2009) 12573.
[57] K.A. Peterson, D. Figgen, E. Goll, H. Stoll, M. Dolg, J. Chem. Phys. 119 (2003) 11113.
[58] J. Oomens, B.G. Sartakov, G. Meijer, G. von Helden, Int. J. Mass Spectrom. 254 (2006) 1.
[59] J. Banisaukas, J. Szczepanski, J.R. Eyler, M. Vala, S. Hirata, M. Head-Gordon, J. Oomens, G. Meijer, G. von Helden, J. Phys. Chem. A 107 (2003) 782.
[60] A. Fielicke, R. Mitric, G. Meijer, V. Bonacic-Koutecky, G. von Helden, J. Am. Chem. Soc. 125 (2003) 15716.
[61] J.B. Foresman, A.E. Frisch, Exploring Chemistry with Electronic Structure Methods, Gaussian, Pittsburgh, PA, 1996.
[62] S.R. Langhoff, J. Phys. Chem. 100 (1996) 2819.
[63] G.S. Groenewold, K.C. Cossel, G.L. Gresham, A.K. Gianotto, A.D. Appelhans, J.E. Olson, M.J. Van Stipdonk, W. Chien, J. Am. Chem. Soc. 107 (2006) 3075.
[64] G.S. Groenewold, A.K. Gianotto, K.C. Cossel, M.J. Van Stipdonk, J. Oomens, N. Polfer, D.T. Moore, W.A. de Jong, M.E. McIlwain, Phys. Chem. Chem. Phys. 9 (2007) 596.